IOPscience iopscience.iop.org

Home Search Collections Journals About Contact us My IOPscience

Monitoring Wind Turbine Loading Using Power Converter Signals

This content has been downloaded from IOPscience. Please scroll down to see the full text.

2016 J. Phys.: Conf. Ser. 749 012018

(http://iopscience.iop.org/1742-6596/749/1/012018)

View the table of contents for this issue, or go to the journal homepage for more

Download details:

IP Address: 129.234.252.67
This content was downloaded on 10/10/2016 at 15:27

Please note that terms and conditions apply.

You may also be interested in:

Model Wind Turbines Tested at Full-Scale Similarity
M.A. Miller, J. Kiefer, C. Westergaard et al.

A numerical study on the flow upstream of a wind turbine in complex terrain
A R Meyer Forsting, A Bechmann and N Troldborg

Calculating the sensitivity of wind turbine loads to wind inputs using response surfaces
Jennifer M. Rinker

Investigations into the Interaction of a Wind Turbine with Atmospheric Turbulence in Complex Terrain
C Schulz, L Klein, P Weihing et al.

Prediction of dynamic strains on a monopile offshore wind turbine using virtual sensors
A N Iliopoulos, W Weijtjens, D Van Hemelrijck et al.

Vector control of wind turbine on the basis of the fuzzy selective neural net*
E A Engel, I V Kovalev and N E Engel

Ice Accretion Prediction on Wind Turbines and Consequent Power Losses
Ozcan Yirtici, Ismail H. Tuncer and Serkan Ozgen

Monitoring Wind Turbine Loading Using Power Converter Signals

C A Rieg[1], **C J Smith**[1], **C J Crabtree**[1]

[1]School of Engineering and Computing Sciences, Durham University, Lower Mountjoy, South Road, Durham, DH1 3LE, UK

c.j.crabtree@dur.ac.uk

Abstract. The ability to detect faults and predict loads on a wind turbine drivetrain's mechanical components cost-effectively is critical to making the cost of wind energy competitive. In order to investigate whether this is possible using the readily available power converter current signals, an existing permanent magnet synchronous generator based wind energy conversion system computer model was modified to include a grid-side converter (GSC) for an improved converter model and a gearbox. The GSC maintains a constant DC link voltage via vector control. The gearbox was modelled as a 3-mass model to allow faults to be included. Gusts and gearbox faults were introduced to investigate the ability of the machine side converter (MSC) current (I_q) to detect and quantify loads on the mechanical components. In this model, gearbox faults were not detectable in the I_q signal due to shaft stiffness and damping interaction. However, a model that predicts the load change on mechanical wind turbine components using I_q was developed and verified using synthetic and real wind data.

1. Introduction

Extreme wind conditions such as gusts can lead to very large loads on the turbine that cause fatigue, shut-downs and damage to components such as the gearbox [1]. In response the condition of wind turbine components is monitored so that a developing fault can be detected and appropriate action taken. This allows maintenance to be scheduled before the impact on the system has become too large, resulting in lower downtimes and lower cost of energy (CoE) [2].

Condition monitoring (CM) techniques such as vibration and strain measurement require expensive sensors that are often impractical in the high-torque applications of wind turbines [3]. Using readily available signals from other areas of the turbine could prove an inexpensive alternative CM approach.

The power converter could provide this information for CM applications; the converter should respond to any disturbances and therefore its signals should show the drive train response. For example, the quadrature-axis component of the machine side converter (MSC) current signal (I_q) controls the real power flow and contains torsional information from the drive train. Monitoring I_q could provide useful information about torsional loads on components that could be used for early fault detection without extra sensors.

This investigation focuses on whether power converter signals can be used for CM with a focus on two potential applications:

1. Gear tooth failure detection.
2. Mechanical load estimation from damaging gusts.

Content from this work may be used under the terms of the Creative Commons Attribution 3.0 licence. Any further distribution of this work must maintain attribution to the author(s) and the title of the work, journal citation and DOI.
Published under licence by IOP Publishing Ltd

2. Approach

To carry this work out a drive train model was required. The model developed at Durham in Simulink [4] was used. It is a drivetrain model of a fully rated, direct-drive 2MW permanent magnet synchronous generator (PMSG) wind turbine with two voltage sources connected to ground simulating the DC link. To make this model suitable for this study the following modifications were made:

1. A full grid-side converter (GSC) was added for a more realistic converter model.
2. A gearbox was added.
3. A gearbox fault model was used to provide fault conditions.
4. A gust model was added to provide data for load prediction.

A schematic of the final model is shown in figure 1. This section outlines how these aspects were modelled. Modifications to the PMSG and MSC as a result of including a gearbox are also detailed.

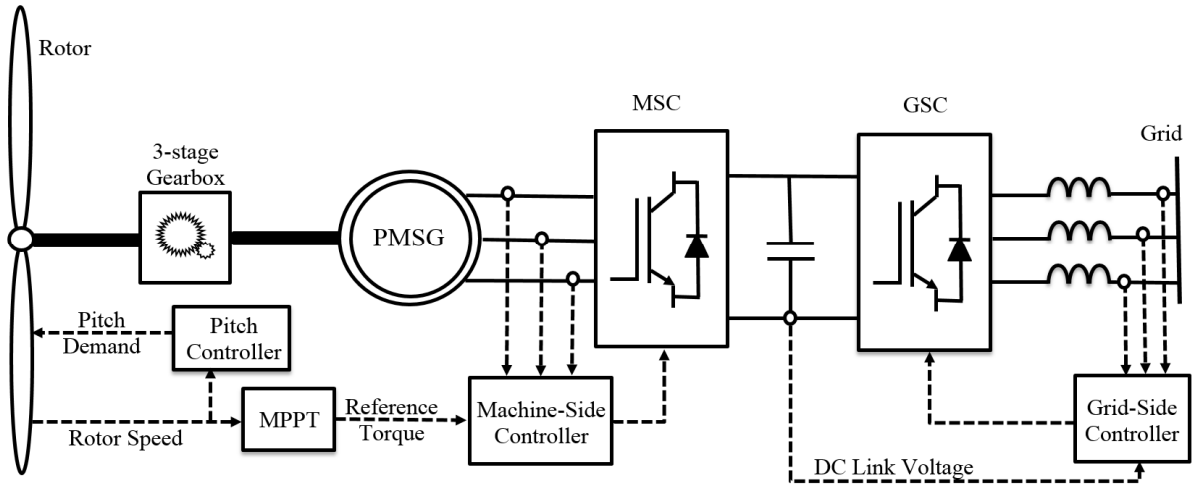

Figure 1. Schematic of the 2MW geared PMSG wind energy conversion system. MPPT stands for maximum power point tracking.

2.1. Grid-Side Converter

The main objective of the GSC is to control power flow between converter and grid to maintain a constant DC link voltage regardless of the power input from the MSC (figure 1). In this configuration the GSC acts as an inverter and the MSC acts as a rectifier. The GSC was modelled as a 2-level insulated-gate bipolar transistor (IGBT)/diode pair active inverter. In the model the 'Universal Bridge' block from the Simulink library was used with the power electronic device set to 'IGBT/Diodes'. It is controlled using the 'PWM Generator (2 level)' block that takes the voltage from the grid side controller as the modulating input signal. The DC-link voltage is $1150V_{DC}$. The grid is represented as ground connected to a three phase programmable voltage source connected to the GSC via inductors.

To control the GSC, vector control was chosen as it is able to respond to transient events more robustly than load angle control [5]. Figure 2 outlines the control schematic for the GSC. I_d is the direct-axis current, V_d is the direct-axis voltage, ω is the grid frequency (rad/s), L is the grid inductance, V_{DC_link} is the DC-link voltage, V_q is the quadrature-axis voltage, $V_{d,r}$ is the converter reference V_d, $V_{q,r}$ is the converter reference V_q, and V_0 is the 0-component voltage. To convert between 3-phase sinusoidal and direct-quadrature-zero (dq0) reference frames the Park and inverse Park transforms were used.

2.2. Gearbox Model

The gearbox is connected to the hub via the low-speed shaft and to the generator via the high-speed shaft. It increases the speed of the incoming turbine speed to the desired generator speed while reducing the torque by a gear ratio N_{GB}. The dynamic interactions of the rotor, gearbox and generator

were modelled as a 3-mass model. Higher order models were considered, however no data was found and the 3-mass model represents the dynamic interactions of the rotor, gearbox and generator adequately for this project. The 3-mass model is shown in figure 3. J_R is the rotor moment of inertia, J_{GB} is the gearbox moment of inertia, $J_{m1,2}$ are the equivalent moments of inertia for the low and high speed gear sections respectively, $T_{m1,2}$ are the equivalent mechanical torques for the low and high shafts respectively and J_g is the generator moment of inertia.

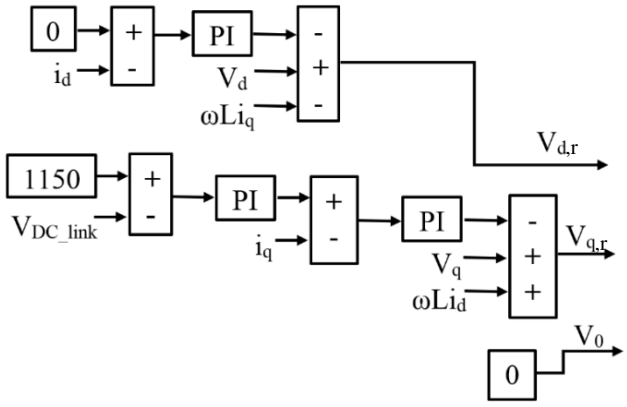

Figure 2. Vector control scheme for the GSC.

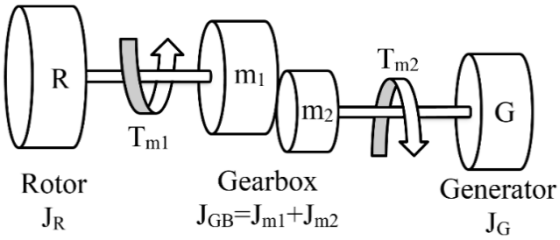

Figure 3. Schematic of the 3-mass model dynamics.

The first mass in the rotor, the second mass is the gearbox and the third mass is the generator. The model uses the principles of a mass-spring-damper system where each mass has inertia J and each shaft a stiffness K and viscous damping B. The second mass (gearbox) is divided into two parts that are related through N_{GB} to represent the difference in speeds of each gear. As such the resulting $T_{m1,2}$ and rotational speeds of the various components (ω) can be represented using equations (1-6).

$$T_{m1} = B_1(\omega_r - \omega_{m1}) + K_1\int(\omega_r - \omega_{m1})\mathrm{d}t \tag{1}$$

$$T_{m2} = B_2\left(\omega_{m2} - \omega_g\right) + K_2\int\left(\omega_{m2} - \omega_g\right)\mathrm{d}t \tag{2}$$

$$\omega_r = \int\frac{T_r - T_{m1}}{J_r}\mathrm{d}t \tag{3}$$

$$\omega_{m1} = \int\frac{T_{m1} - T_g N_{GB}}{J_{GB}}\mathrm{d}t \tag{4}$$

$$\omega_{m2} = \int\frac{T_{m2} - T_r / N_{GB}}{J_{GB}}\mathrm{d}t \tag{5}$$

$$\omega_g = \int\frac{T_e - T_{m2}}{J_g}\mathrm{d}t \tag{6}$$

Where $B_{1,2}$ are the viscous damping of the low and high-speed shaft respectively, $K_{1,2}$ are the shaft stiffnesses of the low and high-speed shafts respectively, ω_r is the rotational speed of the rotor, $\omega_{m1,2}$ are the rotational speeds of the low and high-speed gear components respectively, ω_g is the generator rotational speed. T_r is the rotor torque, T_g is the generator torque, and T_e is the electromechanical torque.

The torque and speed across the rotor and generator are related through the gearbox ratio, N_{GB} using equation (7).

$$N_{\mathrm{GB}} = \frac{\omega_{\mathrm{g}}}{\omega_{\mathrm{t}}} = \frac{T_{\mathrm{r}}}{T_{\mathrm{e}}} \tag{7}$$

Due to the new torque and speed in the generator from [4], changes of the PMSG were made to accommodate the current and voltage requirements. To keep the current and voltage outputs the same equations (8) and (9) were used. The number of poles was reduced to 4 because the generator has a rotational speed of 1500rpm. The flux density was changed to 1.611Vs and the armature inductance was changed to 0.4mH.

$$I_{\mathrm{q}} = \frac{4T_{\mathrm{m2}}}{3p\varphi} \tag{8}$$

$$V_{\mathrm{d},m} = L_{\mathrm{d}}\omega I_{\mathrm{q}} - I_{\mathrm{q}}R_{\mathrm{s}} \tag{9}$$

p is the number of generator poles, φ is the generator flux linkage, $V_{d,m}$ is the MSC direct-axis voltage, L_d is the direct-axis generator inductance, and R_s is the stator resistance. The data for the 3-mass model has been taken from research papers and is given in Appendix B.

2.3. Gearbox Fault Model

The most severe gearbox failure modes that arise from extreme wind conditions have been identified as fretting corrosion and high cycle bending fatigue [6]. Fretting corrosion is the deterioration of contacting gear tooth surfaces as a result of vibratory motion between teeth and is this study's focus.

The gear friction coefficient varies according to three different types of surface structure: adhesion, unevenness and wear [7]. Friction losses in the gears are part of the normal force exerted by each gear at the point of contact F_{N} as a friction factor μ. Due to difficulties involved in the estimation of the μ with lubrication it is often assumed constant [8] and was not used in this project due to a lack of relevant experimental data in the literature. As gears are well lubricated this assumption was deemed satisfactory.

Instead, the gear wear impact on stiffness was considered. The effect of tooth wear on the mechanics of the system has previously been examined and it was found that gear tooth wear causes a reduction in the stiffness of the gear. It was found that it can be modelled as a rectangular pulse wave or a half sine function. The half sine wave function is used in detailed gearbox models that include the gear meshing process in their calculations [9]. For this model the rectangular pulse function was chosen as it represents the fault accurately for the purpose of this investigation.

The reduction of the gear tooth stiffness can be calculated according to equation (10).

$$K_{\mathrm{wear}} = K_{\mathrm{g}} l_{\mathrm{w}} A \tag{10}$$

Where K_{wear} is the wear stiffness, K_{g} is the hertz contact stiffness, l_{w} is the wear length and A is the amplitude of wear.

Typical values of l_{w} are between 1 and 2mm and A typically has a value between 0 and 1 [9]. The contact stiffness with a wear fault present, $K_{\mathrm{g,wear}}$, is given as the difference between the non-faulty gear stiffness and the wear stiffness as in equation (11) [9].

$$K_{\mathrm{g,wear}} = K_{\mathrm{g}} - K_{\mathrm{wear}} \tag{11}$$

The relationship between the contact stiffness of the gears and the stiffness of the shaft can be modelled as springs connected in series. The total stiffness K_{Total} is calculated from K_{g} and the shaft stiffness K_{S} as in equation (12).

$$K_{\mathrm{Total}} = \frac{1}{\frac{1}{K_{\mathrm{g}}} + \frac{1}{K_{\mathrm{s}}}} \tag{12}$$

The effect of tooth wear in the gearbox was modelled as a reduction in the total stiffness every time there is contact with a worn gear tooth as shown in figure 4. The total stiffness is applied across the shaft in the model.

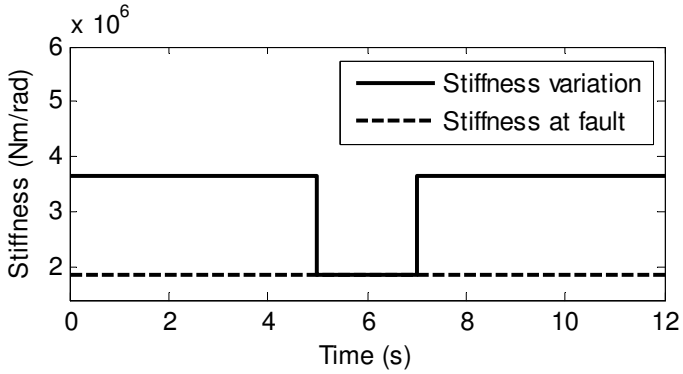

Figure 4. The stiffness relationship in a worn gear.

Other faults such as gear cracks have been modelled using a periodic cosine based variation in shaft stiffness given in (13) where K_{crack} is the reduction in shaft stiffness due to the crack that can be calculated using finite element analysis [9, 10]. The underlying calculations for a crack fault and a wear fault are very similar as they both rely on a periodic reduction in the shaft stiffness due to a fault.

$$K_{\text{s}} = \frac{1-\cos(\omega t)}{2} K_{\text{crack}} \tag{13}$$

Gearbox faults are often modelled as a periodic variation in tooth stiffness to indicate the presence of a fault. As a widely used, well-established method of modelling faults and experimental data available, it was chosen in this project.

A typical gearbox in a wind turbine has 3-stages with a planetary gearbox at the first stage, coupled to two parallel gearboxes at the second and third stage [11]. Due to the speed dependency of the gear fault model, faults can be introduced into any of the gear stages. Appendix A gives a summary of the gear ratios and output speeds corresponding to the individual stages.

2.4. Gust Model

Existing gust models rely on real wind data to model the amplitude, duration and gust shape introduced along with a running average wind speed [12, 13]. These wind gust profile characteristics can be extracted and applied using square or cosine shaped wind profiles that have a gust amplitude, duration and frequency. The maximum gust speed ($U_{\text{G,max}}$) in a given time period is calculated from the gust factor *G(t)* in equation (14). An expression for the gust factor is given in equation (15) [14].

$$U_{\text{G,max}} = G(t) U_{\text{W}} \tag{14}$$

$$G(t) = 1 + 0.42 I_{\text{u}} \log_{\text{e}}\left(\frac{3600}{t_G}\right) \tag{15}$$

Where U_w is the mean wind speed, I_{u} is the longitudinal turbulence intensity, and t_G is the gust duration.

The International Electrotechnical Commission (IEC) has divided the value for turbulence intensity into three categories - higher, medium and lower turbulence characteristics with values of 0.16, 0.14 and 0.12 respectively [15]. The underlying square wave gust characteristic was used as the basis for all gust analysis.

For the load prediction model gust, 10 gust categories were defined, each representing a reduction in the gust wind speed (table 1).

Table 1. Gust category assignment.

Gust Category	U_G	Gust Category	U_G
1	$(U_G+U_W) + U_W$	6	$[(U_G + U_W)/2.25] + U_W$
2	$[(U_G + U_W)/1.25] + U_W$	7	$[(U_G + U_W)/2.5] + U_W$
3	$[(U_G + U_W)/1.5] + U_W$	8	$[(U_G + U_W)/3] + U_W$
4	$[(U_G + U_W)/1.75] + U_W$	9	$[(U_G + U_W)/4] + U_W$
5	$[(U_G + U_W)/2] + U_W$	10	$[(U_G + U_W)/6] + U_W$

3. Results

The section presents and discusses the results of gearbox fault detection using converter signals (section 3.1), and estimating turbine drive train loads from gusts using converter signals (section 3.2).

3.1. Gearbox Fault Detection

Gearbox wear faults were introduced using the method outlined in section 2.3. The first fault was introduced as a wear fault with wear amplitude 0.5 and wear length 1mm present on every other tooth, giving a fault frequency of 1.72Hz. The incoming wind speed was constant at 7m/s. The parameters used to introduce the first fault in the second gearbox stage of the gearbox are detailed in Appendix B.

By taking the Fast Fourier Transform (FFT) of the MSC I_q signal the frequency spectrum was computed to identify differences between the 'healthy' (no fault) and faulty spectrum. Figure 5 shows the frequency response of the MSC I_q signal in its 'healthy' and faulty state as well as the amplitude difference between the healthy and faulty state. It can be seen that there is no clear difference in the spectrum at the fault frequency. There is a small difference at 2Hz, where both the healthy and the faulty spectrum show a spike due to control errors.

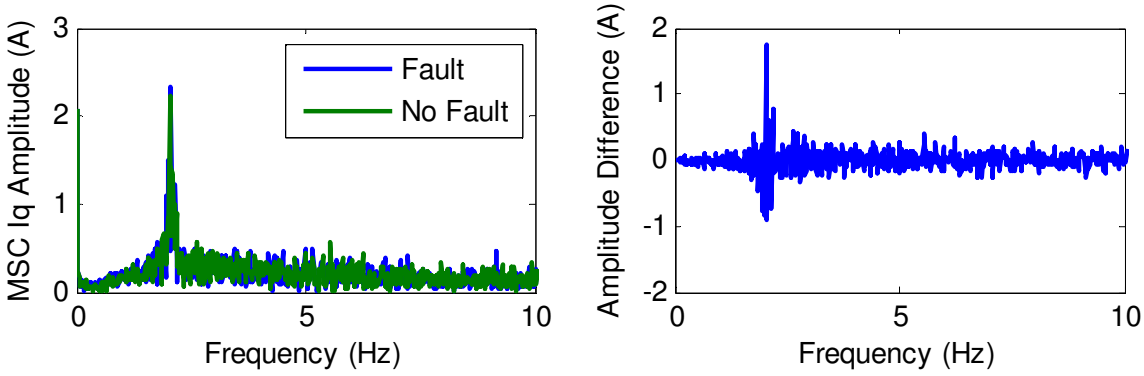

Figure 5. MSC I_q frequency response

It was investigated why the fault does not appear in the MSC I_q frequency spectrum by looking at the frequency spectrum of the relevant torque components. The torque across the high speed shaft is an input to the PMSG and is used to determine the MSC I_q and is result of the addition of the torque due to stiffness (T_K) and the torque due to damping (T_B). Figure 6 shows the frequency spectrum of each of these individual torque signals in their 'healthy' state and their faulty state. It can be seen that the fault is visible in the frequency spectrum of T_K and T_B (figure 6), yet is no longer visible in the resulting total torque spectrum (figure 5).

To understand the impact of the damping and stiffness components on the fault frequency response, the time sequence of T_K and T_B was monitored with the fault present (figure 7). The time sequences showed that the oscillatory motion of T_K due to the fault is counteracted by an opposite oscillatory motion from T_B removing the oscillation due to the fault from the frequency spectrum.

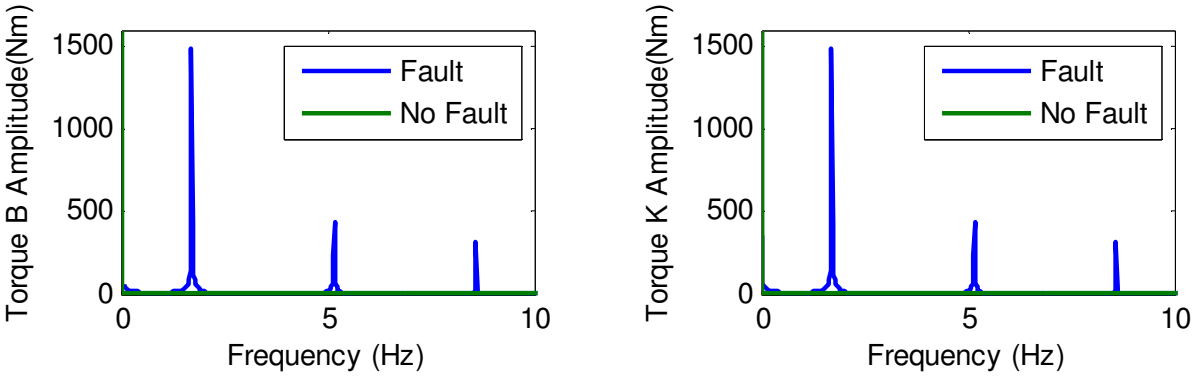

Figure 6. Frequency spectrum of mechanical torque components.

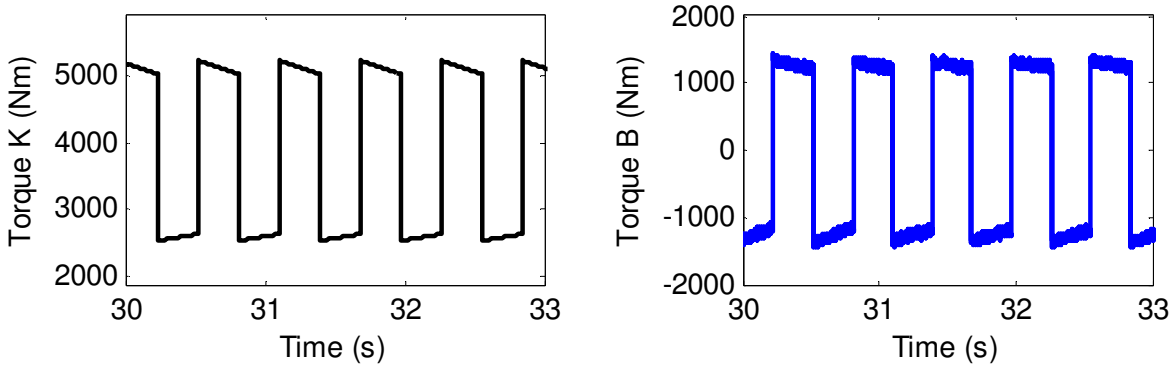

Figure 7. Temporal spectrum of mechanical torque components.

The amplitude of the torque due to damping counteracts the amplitude of the torque due to stiffness exactly, resulting in a critically damped system. The gearbox was modelled analogous to a mass-spring-damper system. In this system the role of the damper is to reduce or prevent oscillations. The fault amplitude was varied in the full range of 0 to 1 and the wear length was varied in the full range of 1mm to 2mm and the input speed was varied. However in each case the system remained critically damped, resulting in the fault not appearing in the MSC signals.

In a real gearbox the torque due to damping and torque due to stiffness cannot be measured separately as they have been in this model. In a real gearbox the system parameters might not be as perfectly balanced as in this modelled system and the damping might not have the same effect as in this model. Thus there is a possibility that faults can be detected in the MSC I_q signal of a real gearbox system where the components and parameters are not as balanced as in this drive train model.

3.2. Load prediction on mechanical components using MSC signals

The MSC converter signal spectrum changes with the incoming wind speed and wind pattern. Wind gusts at varying frequencies appear clearly on the spectrum and can be monitored using the MSC signals. Figure 8 shows the variation of the frequency spectrum as the gust frequency of the incoming wind is varied at a mean wind speed of 7.5 m/s using the maximum gust speed.

Simulations were done at different speeds and constant gust frequency of 3Hz. A relationship between the MSC I_q amplitude and the difference in rotor torque magnitude was derived for each gust category using simulation results as data points. The result for the first, second and third gust categories are shown in Figure 9 with equations (16-18) representing their relationship respectively. ΔT_r is the change in mechanical load on the rotor in kNm.

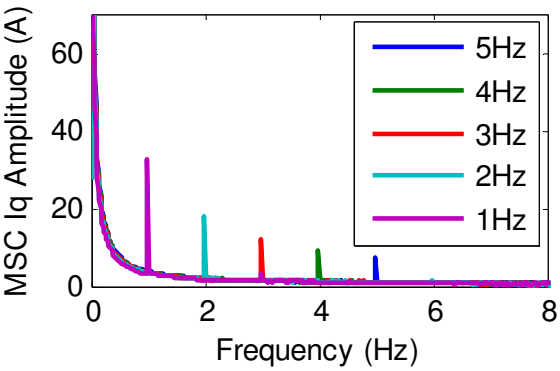

Figure 8. MSC I_q frequency spectrum for different gust frequencies.

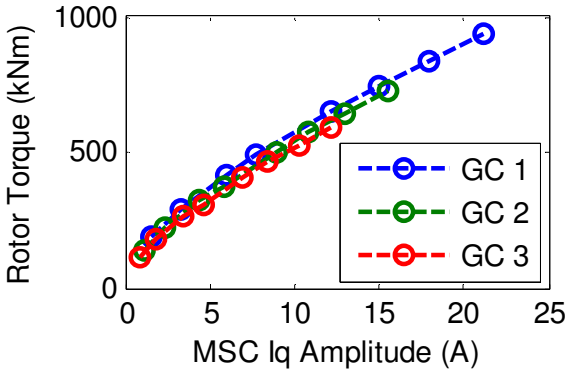

Figure 9. ΔT_r vs MSC I_q amplitude for different gust categories.

$$\text{GC 1: } \Delta T_r = 137.7 I_q^{0.6238} \tag{16}$$

$$\text{GC 2: } \Delta T_r = 130.21 I_q^{0.6206} \tag{17}$$

$$\text{GC 3: } \Delta T_r = 123.92 I_q^{0.6176} \tag{18}$$

With this information, a load prediction model can be constructed. The proposed model works on the basis that the wind speed and MSC signal amplitudes can be measured. A flowchart of its operating principle is illustrated in Figure 10. The wind is monitored and depending on the mean wind speed and gust magnitude it can be assigned a gust category. Each gust category has an equation relating the change in torque and the MSC current amplitude for an assigned frequency range.

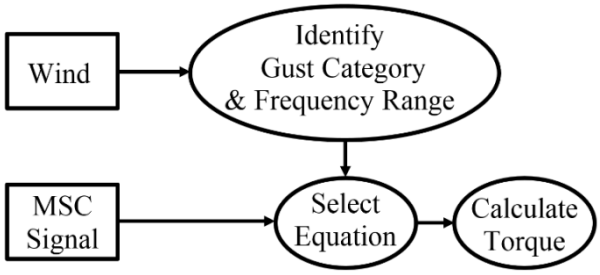

Figure 10. Flowchart of the load prediction model.

Depending on the gust category and gust frequency, an equation is selected from which ΔT_r can be calculated. The frequency ranges become smaller as the gust frequency decreases because the change in I_q amplitude increases. Severe load changes can then be counted to estimate the mechanical fatigue.

In order to verify the functionality of this method a variety of ideal category 1 gusts with different mean wind speeds were inputted into the model. The MSC I_q FFT amplitude was measured and the expected load on the rotor was calculated according to equation ($\Delta T_{r,est}$) (16). $\Delta T_{r,est}$ was compared to the measured torque from the simulation ($\Delta T_{r,sim}$) using the percentage error.

The results are summarised in table 2. The percentage error between the measured and the calculated error is very small, below 1%. This shows that the model is able to predict the load on the mechanical components in the wind turbine drive train through MSC signal measurements adequately.

The model was tested using real wind data from the anemometer on a 1.5MW variable speed wind turbine in order to investigate the accuracy of the model using a real, non-ideal wind characteristic. The data was identified as GC 10 and frequency 0.29Hz. The equation relating $\Delta T_{r,est}$ and MSC I_q in this case is given by (19). Table 2 gives a summary of the results.

Table 2. Model Verification and response to real wind input.

U_W (m/s)	MSC I_q (A)	$\Delta T_{r,est}$ (Nm)	$\Delta T_{r,sim}$ (Nm)	% Error
		Verification (GC 1)		
5.5	4.536	353636.5	350370	0.92
6.2	6.648	448868.5	445450	0.76
7	9.84	573264.2	568160	0.89
8.2	16.344	786715	780330	0.81
		Real wind input (GC 10)		
8.4	11.82	98978.5	104860	5.9

$$\Delta T_{r,est} = 15.739 I_q^{0.7445} \tag{19}$$

The percentage error for the real wind is higher than for the ideal wind. This is expected as the real wind gusts have a larger variation in duration and magnitude. The frequency of the gusts in the real wind characteristic is not as clear as in the ideal characteristic. The frequency categories allow for some variation that increases the percentage error. For a mean wind speed of 8.5m/s with gusts of frequency 0.29Hz the difference between the maximum (GC 1) and minimum (GC 10) change in rotor torque is 555910Nm. The difference between the calculated and measured rotor torque from Table 3 is 5881.9Nm, which is 100 times smaller than the difference between GC1 and GC10. This indicates that the model has the ability to estimate the change in load using real wind characteristics well.

4. Conclusion

CM of wind turbine components allows appropriate action to be taken to minimise the impact of developing faults but currently requires expensive sensors and data acquisition devices**.** This paper investigates whether converter signals, which are already monitored by turbine controllers, can be used for CM.

A drive train model was modified to include a gearbox, GSC and gearbox fault model to determine whether gearbox faults could be detected in the converter signals. Gusts were also modelled to determine if drive train mechanical loading could be predicted using converter signals. The conclusions from this study are:

- Gear wear cannot be detected in the MSC signals due to the model damping effects. However, physical testing should be carried out to explore the impact of non-ideal dynamics.
- A model using MSC signals successfully predicted the load changes in the turbine with a percentage error < 1% under ideal wind conditions, and <6% for a real wind speed case.

Further investigations into the magnitude of load changes that cause mechanical component damage could lead to the application of this accurate MSC-based load prediction model to prevent gearbox faults through turbine shutdown during damaging wind conditions.

Appendices

Appendix A. 3-stage gearbox gear ratios.

	Stage 1	Stage 2	Stage 3
Gear type	Planetary	Parallel	Parallel
Gear ratio	1:16.667	1:2	1:2
Output speed	375rpm	750rpm	1500rpm

Appendix B. Data for 3 mass model and gear faults.

Parameter	Value	Ref	Parameter	Value	Ref
J_r	$2.92\text{x}10^6$ kgm^2	[16]	K_2	$2.29\text{x}10^8$ Nm/rad	[18]
J_g	200 kgm^2	[17]	K_g	$3.715\text{x}10^6$ Nm/rad	[17]
J_{GB}	190 kgm^2	[17]	K_{wear}	1857.5 Nm/rad	(10)
B_1	6.72 Nms/rad	[4]	$K_{g,wear}$	3713143Nm/rad	(11)
B_2	6.72 Nms/rad	[4]	K_{Total}	3655585 Nm/rad	(12)
K_1	$4.00\text{x}10^7$ Nm/rad	[16]	$K_{Total,wear}$	1842070 Nm/rad	(12)

References

[1] Kanev S and van Engelen T 2010 Wind turbine extreme gust control *Wind Energy* **13** pp 18-35
[2] Han Y and Song Y 2003 Condition monitoring techniques for electrical equipment-a literature survey *IEEE Trans. Power Del.* **18**(1) pp 4-13
[3] Yang W, Tavner P, Crabtree C and Wilkinson M 2010 Cost-effective condition monitoring for wind turbines *IEEE Trans. Ind. Electron*. **57**(1), pp 263-71
[4] Smith C, Wadge G, Crabtree C and Matthews P 2015 Characterisation of electrical loading experienced by a nacelle power converter *EWEA Annual Event 17-20 Nov. (Paris)*
[5] Anaya-Lara O, Jenkins N, Ekanayake J, Cartwright P and Hughes M 2009 *Wind Energy Generation: Modelling and Control* (West Sussex: Wiley)
[6] Sheng S and McDade M 2011 Wind turbine failure modes *IJTC 23-26 Oct. (Los Angeles)*
[7] Mahdavian S and Mai Y 1984 Further study in friction, metallic transfer and wear debris of sliding surfaces *Wear* **95** pp 35-44
[8] Brethee K, Gao J, Gu F and Ball A 2015 Analysis of frictional effects in the dynamic response of gear systems and the implications for diagnostics *ICAC 11-12 Sep. (Glasgo*w)
[9] Cui L and Cai C 2015 Nonlinear Dynamics of a Gear-Shaft-Bearing System Breathing Crack and Tooth Wear Faults *Open Mech J* **9** pp 483-491
[10] Kidar T, Thomas M, El Badaoui M and Guibault R 2013 Control of phases by ESPRIT and WLSE methods for the early detection of gear cracks *3rd International Congress on Engineering Industrial Risk 3-5 Jul. (Riems)*
[11] Feng Y, Li J, Qiu Y, Yang W and Infield D 2014 Study on order analysis for condition monitoring wind turbine gearbox *RPG 24-25 Sep. (Naples)*
[12] Sheridan P 2011 Review of techniques and research for gust forecasting and parameterization *Forecasting Research Technical Report 570* (Exeter: Met Office)
[13] Verheij F, Cleijne J and Leene J 1992 Gust modelling for wind loading *J WIND ENG IND AEROD* **42**(1-3) pp 947-958
[14] Burton T, Jenkins N, Sharpe D and Bossanyi E 2011 *Wind energy handbook* (West Sussex: Wiley).
[15] IEC 2005 Wind turbines-Part 1: design requirements *IEC 61400-1:2005(E)*
[16] Akhmatov V 2003 Analysis of dynamic behaviour of electric power systems with large amount of wind power *Electric Power Engineering Ørsted-DTU Thesis*
[17] Jiang B 2010 Modelling of dynamics of driveline of wind stations *Chalmers University of Technology Master's Thesis*
[18] Ackermann T 2005 *Wind power in power systems* (West Sussex: Wiley)